ROYAL SOCIETY OF CHEMISTRY

PAPER

Check for updates

Rational molecular engineering of porphyrins for enhanced performance in dye-sensitized solar cells†

Faraghally A. Faraghally,‡[a] Yu-Hsuan Chen, [iD] ‡[b] Tsung-Zu Lee,[b] Yan-Da Chen,[b] Tzu-Chien Wei [iD] *[a] and Chen-Yu Yeh [iD] *[b]

Porphyrin dyes are promising sensitizers for high-efficiency dye-sensitized solar cells (DSSCs) due to their remarkable light-harvesting capabilities. However, realizing their full potential in photovoltaic devices necessitates meticulous optimization of their molecular structure. This study explores the structure–performance relationship in nine novel porphyrin dyes (**TZ1–TZ9**), aiming to enhance the overall power conversion efficiency (PCE). The impact of donor ability and its bulkiness is investigated using bis(4-hexylphenyl)amine and a bulky modified Hagfeldt donor (bis(2′,4′,6′-tris(hexyloxy)-[1,1′-biphenyl]-4-yl) amine). Indacenodithiophene IDT and thiophene groups are also incorporated as π-spacers to improve the light-harvesting efficiency and increase the overall molecular bulkiness. Furthermore, diverse acceptors (benzothiadiazole, benzotriazole, and cyanoacrylic acid) are introduced to fine-tune photophysical and electrochemical properties. Among these porphyrin dyes, **TZ1** exhibits a remarkable PCE of 9.90% (short circuit photocurrent (J_{SC}) = 15.675 mA cm^{-2}, open circuit photovoltage (V_{OC}) = 0.834 V, and fill factor (FF) = 0.758), surpassing the PCE of 9.20% (J_{SC} = 14.737 mA cm^{-2}, V_{OC} = 0.817 V, and FF = 0.764) achieved by **GY50** under similar fabrication conditions.

1. Introduction

Driven by escalating fossil fuel depletion and intensifying environmental concerns, the quest for sustainable energy solutions has become a paramount global challenge. Among renewable energy technologies, solar energy stands out as a frontrunner.[1–4] In this context, dye-sensitized solar cells (DSSCs) have attracted significant interest within the scientific community as a promising technology for future renewable energy systems. This heightened interest stems from their advantageous attributes, encompassing a cost-effective, solution-based fabrication process, a demonstrably minimal environmental impact, and the remarkable ability to show excellent efficiency under low-light conditions.[5–12]

Crucially, the sensitizer within a DSSC plays a significant role in capturing solar energy and facilitating its conversion into an electric current. Among the sensitizer types employed in DSSCs (Organic dyes, ruthenium complexes, porphyrins, and natural dyes),[8,13,14] porphyrin dyes hold significant promise due to their unique properties. These include intense light absorption across the visible spectrum, readily available constituent elements, robust thermal stability, and the ability to tailor their electrochemical properties through molecular engineering.[15,16]

The meticulous design of porphyrin sensitizers plays a vital role in maximizing the power conversion efficiency (PCE) of DSSCs. To achieve this objective, strategic manipulation of the donor, π-conjugated spacer, and acceptor moieties within the porphyrin scaffold, particularly at the *meso* and β-positions, is essential. These modifications enable better energy level alignment, enhancing the efficient transfer of charge within the molecule. Consequently, improving the light-harvesting efficiency (LHE) and optimized charge dynamics are facilitated within the DSSC architecture.[15–22] Additionally, incorporating sterically hindered substituents strategically suppresses dye aggregation and reduces charge recombination, thus contributing significantly to the long-term stability and sustained performance of DSSCs.[21,23–31]

However, early porphyrin-based exhibited low device performance until the **YD** series of porphyrins was introduced.[32–36] The **YD**-series of porphyrins, featuring D–π–A molecular design, boosted both the electron injection efficiency and the light-harvesting, enabling **YD2** to achieve a PCE of 11%.[37] This advancement paved the way for the synthesis of

[a] *Department of Chemical Engineering, National Tsing Hua University, Hsinchu City 30044, Taiwan. E-mail: tcwei@mx.nthu.edu.tw*

[b] *Department of Chemistry, i-Center for Advanced Science and Technology (i-CAST), Innovation and Development Center of Sustainable Agriculture (IDCSA), National Chung Hsing University, Taichung City 402, Taiwan. E-mail: cyyeh@dragon.nchu. edu.tw*

† Electronic supplementary information (ESI) available: It includes the synthesis procedures, ^{1}H NMR spectra, ^{13}C NMR spectra, mass spectra, details of theoretical calculations and all necessary figures and tables of the new compounds. See DOI: https://doi.org/10.1039/d5se00043b

‡ F. A. Faraghally and Y.-H. Chen contributed equally to this work.

YD2-*o*-C8, an ingeniously designed derivative incorporated with judiciously tailored alkoxy chains. These modifications demonstrably suppressed dye aggregation and mitigated interfacial back electron transfer, resulting in a noteworthy PCE of 11.9% under AM 1.5G irradiation.[25] Furthermore, **GY50** dye was obtained by incorporating an electron-withdrawing benzothiadiazole (**BTD**) moiety between the core of porphyrin and the anchoring group. This strategic enhancement extended conjugation and heightened intramolecular charge transfer (ICT), resulting in an impressive PCE of 12.8%.[17] Subsequently, the development of **SM315** involved the integration of a bulky donor moiety, bis(20,40-bis(hexyloxy)-[1,10-biphenyl]-4-yl)amino group, culminating in a remarkable PCE of 13%.[26] A recently developed double-fence porphyrin dye incorporated strategically positioned alkoxyl groups at the *ortho*-positions of its phenyl rings mitigated charge recombination and diminished the dye aggregation.[38] Continuing this successful design strategy, further research efforts have been directed towards incorporating the Indacenodithiophene (IDT) group within the porphyrin dyes as a donor moiety to achieve enhanced photovoltaic performance. As a result, **YS7**-based devices exhibited an exceptional PCE of 11.4%.[39] Despite the demonstrably successful application of porphyrin dyes in dye-sensitized solar cells (DSSCs), a disparity remains between their achieved efficiencies and the theoretical efficiency of 20% PCE. This disparity underscores the imperative for further investigation into targeted molecular engineering to realize highly efficient and cost-competitive solar cell technologies.

In this respect, we systematically modified the donor, π-spacer, and acceptor moieties within the D–π–A porphyrin framework. This strategic approach enables the investigation of the structure–performance relationship governing the sensitizers, thus enhancing the overall PCE. As illustrated in Fig. 1, nine novel porphyrins (**TZ1–TZ9**) were synthesized and

subsequently employed as DSSC sensitizers. To examine the influence of donor ability and its steric bulk on the performance of DSSCs, we employed two distinct donor types: an alkyl arylamine and a bulky modified Hagfeldt donor incorporating six alkoxy chains.[40] Moreover, to fine-tune the photophysical and electrochemical properties of the dyes, three distinct acceptor units were strategically incorporated: benzothiadiazole (**BTD**), benzotriazole (**BTA**), and cyanoacrylic acid. Finally, the influence of the π-spacer on photovoltaic performance was investigated through two strategies. The first strategy involved incorporating an IDT unit, enhancing π-conjugation and overall molecular bulkiness. The second strategy focused on extending the dye structure by introducing an additional thiophene unit coupled with BTA moiety. This modification aims to enhance the light-harvesting capability, mitigate charge recombination processes, and optimize the dye loading capacity within the DSSC. Among these newly synthesized porphyrin dyes, **TZ1** exhibited a remarkable PCE of 9.90%% ($J_{SC} = 15.675$ mA cm^{-2}, $V_{OC} = 0.834$ V, and FF = 0.758), surpassing the PCE of 9.20% ($J_{SC} = 14.737$ mA cm^{-2}, $V_{OC} = 0.817$ V, and FF = 0.764) achieved by the benchmark **GY50** under identical fabrication conditions. This improvement highlights the crucial role of molecular design in optimizing DSSC performance.

2. Experimental section

2.1 Experimental procedures

The syntheses of precursors (**4**, **9–14**) are described in the ESI.†

2.1.1 Procedure for synthesis of TZ1. To a solution of **1** (100 mg, 0.064 mmol) in THF (10 mL) was added tetra-*n*-butylammonium fluoride solution 1.0 M in THF (0.64 mL, 0.64 mmol). After stirring at room temperature for 10 min, the mixture was extracted with CH_2Cl_2/H_2O. The organic layer was collected and dried over Na_2SO_4, then the solvent was removed
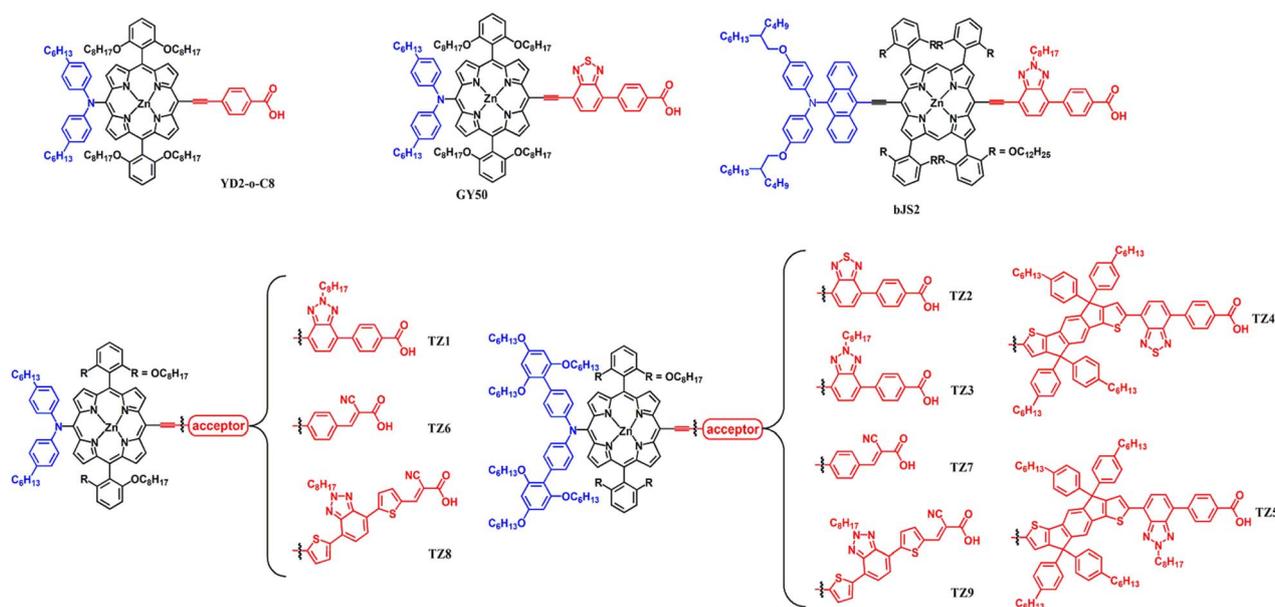

Fig. 1 Chemical structures of **YD2-*o*-C8**, **GY50**, **bJS2**, and **TZ** porphyrin dyes.

under vacuum to afford a crude product of desilylated porphyrin, which was used without further purification. Afterward, a solution of the desialylated porphyrin, **5** (110.0 mg, 0.256 mmol), $Pd_2(dba)_3$ (29 mg, 0.032 mmol), $AsPh_3$ (78 mg, 0.256 mmol), and NEt_3 (1.85 mL, 13.3 mmol) in THF (16 mL) was heated at 85 °C for 12 h. After cooling to room temperature, the catalyst was removed with Celite, and the solvent was removed under reduced pressure. The residue was purified by column chromatography (silica gel) using CH_2Cl_2 as an eluent to give **TZ1** (60 mg, 54%) as a bright green solid. ^1H NMR (400 MHz, $CDCl_3$): δ 9.98 (d, $J = 4.6$ Hz, 2H), 9.18 (d, $J = 4.6$ Hz, 2H), 8.93 (d, $J = 4.6$ Hz, 2H), 8.70 (d, $J = 4.6$ Hz, 2H), 8.33 (d, $J = 8.4$ Hz, 2H), 8.27 (d, $J = 8.4$ Hz, 2H), 8.09 (d, $J = 7.4$ Hz, 1H), 7.85 (d, $J = 7.5$ Hz, 1H), 7.68 (t, $J = 8.4$ Hz, 2H), 0.23 (d, $J = 8.6$ Hz, 4H), 6.99 (d, $J = 8.5$ Hz, 4H), 6.94 (d, $J = 8.6$ Hz, 4H), 5.01 (t, $J = 7.2$ Hz, 2H), 3.95–3.66 (m, 8H), 2.52–2.43 (m, 4H), 2.39 (dt, $J = 14.9$ Hz, 7.4 Hz, 2H), 1.67–1.45 (m, 8H), 1.44–1.09 (m, 22H), 1.09–0.95 (m, 8H), 0.95–0.76 (m, 18H), 0.75–0.57 (m, 25H), 0.57–0.41 (m, 16H). ^{13}C NMR (101 MHz, $CDCl_3$): δ 159.9, 152.3, 151.9, 150.5, 150.4, 150.2, 134.6, 132.2, 132.0, 130.8, 130.6, 130.5, 129.8, 128.7, 128.5, 121.9, 120.8, 114.5, 105.2, 68.6, 57.1, 35.2, 31.8, 31.7, 31.5, 31.4, 30.2, 29.1, 28.6, 28.6, 28.4, 26.7, 25.1, 22.6, 22.2, 14.1, 13.7. MALDI-MS (HRMS): m/z calcd. for $C_{111}H_{140}N_8O_6Zn$: $[M]^+$ 1745.0187; found 1745.0182.

2.1.2 Procedure for synthesis of TZ2. To a solution of **4** (72 mg, 0.034 mmol) in THF (5 mL) was added tetra-n-butylammonium fluoride solution 1.0 M in THF (0.34 mL, 0.34 mmol). After stirring at room temperature for 10 min, the mixture was extracted with CH_2Cl_2/H_2O. The organic layer was collected and dried over Na_2SO_4, then the solvent was removed under a vacuum to afford a crude product of desilylated porphyrin, which was used without further purification. Afterward, to a solution of the desilylated porphyrin, **8** (34.0 mg, 0.102 mmol), $Pd_2(dba)_3$ (15.6 mg, 0.017 mmol), $AsPh_3$ (41.6 mg, 0.136 mmol), and NEt_3 (1 mL, 7.19 mmol) in THF (5 mL) was heated at 85 °C for 12 h. After cooling to room temperature, the catalyst was removed with Celite, and the solvent was removed under reduced pressure. The residue was purified by column chromatography (silica gel) using CH_2Cl_2 as eluent to give **TZ2** (31 mg, 40%) as a yellow-brown solid. ^1H NMR (400 MHz, $CDCl_3$): δ 10.01 (s, 2H), 9.28 (s, 2H), 8.96 (s, 2H), 8.68 (s, 2H), 8.23 (d, $J = 21.3$ Hz, 5H), 7.96 (d, $J = 6.8$ Hz, 1H), 7.67 (d, $J = 7.6$ Hz, 2H), 7.34 (d, $J = 7.1$ Hz, 4H), 7.17 (d, $J = 7.3$ Hz, 4H), 6.99 (d, $J = 7.8$ Hz, 4H), 6.15 (s, 4H), 4.06–3.45 (m, 20H), 1.76 (s, 4H), 1.60 (s, 8H), 1.51–1.40 (m, 4H), 1.40–1.12 (m, 34H), 1.12–0.95 (m, 8H), 0.95–0.84 (m, 8H), 0.78 (s, 20H), 0.70–0.19 (m, 42H). ^{13}C NMR (101 MHz, $CDCl_3$): δ 159.9, 159.3, 157.9, 152.3, 152.1, 150.8, 150.5, 150.3, 131.8, 131.7, 130.4, 129.2, 125.9, 121.2, 121.0, 114.6, 113.4, 105.2, 93.1, 68.7, 68.0, 31.6, 31.4, 31.3, 29.3, 29.0, 28.6, 28.5, 25.7, 25.5, 25.1, 22.6, 22.5, 22.2, 14.0, 13.7. MALDI-MS (HRMS): m/z calcd. for $C_{139}H_{179}N_7O_{12}SZn$: $[M]^+$ 2234.2624; found 2234.2618.

2.1.3 Procedure for synthesis of TZ3. To a solution of **4** (100 mg, 0.047 mmol) in THF (5 mL) was added tetra-n-butylammonium fluoride solution 1.0 M in THF (0.47 mL, 0.47 mmol). After stirring at room temperature for 10 min, the mixture was extracted with CH_2Cl_2/H_2O. The organic layer was

collected and dried over Na_2SO_4, then the solvent was removed under a vacuum to afford a crude product of desilylated porphyrin, which was used without further purification. Afterward, to a solution of the desilylated porphyrin, **5** (80.46 mg, 0.186 mmol), $Pd_2(dba)_3$ (21.4 mg, 0.023 mmol), $AsPh_3$ (57.3 mg, 0.187 mmol), and NEt_3 (2 mL, 15.4 mmol) in THF (10 mL) was heated at 85 °C for 12 h. After cooling to room temperature, the catalyst was removed with Celite, and the solvent was removed under reduced pressure. The residue was purified by column chromatography (silica gel) using CH_2Cl_2 as eluent to give **TZ3** (52 mg, 48%) as a green solid. ^1H NMR (400 MHz, $CDCl_3$): δ 9.98 (s, 2H), 9.29 (s, 2H), 8.93 (s, 2H), 8.68 (s, 2H), 8.31 (d, $J = 14.1$ Hz, 4H), 8.08 (s, 1H), 7.85 (s, 1H), 7.68 (s, 2H), 7.34 (s, 4H), 7.18 (s, 4H), 7.00 (s, 4H), 6.16 (s, 4H), 5.01 (s, 2H), 4.09–3.63 (m, 20H), 2.51–2.24 (m, 2H), 1.88–1.69 (m, 4H), 1.69–1.54 (m, 8H), 1.53–1.11 (m, 48H), 1.10–0.96 (m, 8H), 0.95–0.85 (m, 10H), 0.85–0.70 (m, 20H), 0.70–0.26 (m, 44H). ^{13}C NMR (101 MHz, $CDCl_3$): δ 159.9, 159.3, 157.9, 152.2, 150.8, 150.5, 150.2, 132.0, 131.8, 130.6, 129.7, 128.5, 125.9, 121.2, 121.0, 114.4, 113.5, 105.2, 93.1, 68.7, 68.0, 57.1, 31.8, 31.6, 31.4, 31.3, 30.2, 29.3, 29.1, 29.0, 28.6, 28.5, 26.7, 25.7, 25.5, 25.2, 22.6, 22.5, 22.2, 14.1, 14.0, 13.7. MALDI-MS (HRMS): m/z calcd. for $C_{147}H_{196}N_8O_{12}Zn$: $[M]^+$ 2329.4264; found 2329.4259.

2.1.4 Procedure for synthesis of TZ4. To a solution of **4** (150 mg, 0.071 mmol) in THF (5 mL) was added tetra-n-butylammonium fluoride solution 1.0 M in THF (0.71 mL, 0.71 mmol). After stirring at room temperature for 10 min, the mixture was extracted with CH_2Cl_2/H_2O. The organic layer was collected and dried over Na_2SO_4, then the solvent was removed under vacuum to afford a crude product of desilylated porphyrin, which was used without further purification. Afterward, to a solution of the desilylated porphyrin, **11** (263 mg, 0.212 mmol), $Pd_2(dba)_3$ (32 mg, 0.035 mmol), $AsPh_3$ (86 mg, 0.283 mmol), and NEt_3 (1 mL, 7.19 mmol) in THF (5 mL) was heated at 85 °C for 12 h. After cooling to room temperature, the catalyst was removed with Celite, and the solvent was removed under reduced pressure. The residue was purified by column chromatography (silica gel) using CH_2Cl_2 as eluent to give **TZ4** (100 mg, 45%) as a red solid. ^1H NMR (400 MHz, $CDCl_3$): δ 9.53 (d, $J = 4.7$ Hz, 2H), 9.21 (d, $J = 4.5$ Hz, 2H), 8.80 (d, $J = 4.5$ Hz, 2H), 8.61 (d, $J = 4.7$ Hz, 2H), 8.21 (d, $J = 8.4$ Hz, 2H), 8.08–8.04 (m, 3H), 7.92 (s, 1H), 7.75 (d, $J = 7.4$ Hz, 1H), 7.61 (t, $J = 8.4$ Hz, 2H), 7.57–7.52 (m, 3H), 7.29–7.26 (m, 11H), 7.13–7.09 (m, 13H), 6.92 (d, $J = 8.4$ Hz, 4H), 6.09 (s, 4H), 3.89–3.73 (m, 24H), 2.56 (dd, $J = 15.2$, 5.6 Hz, 10H), 1.71 (t, $J = 7.6$ Hz, 6H), 1.58–1.40 (m, 103H), 1.34–1.22 (m, 55H), 1.16–1.15 (m, 21H), 0.97–0.93 (m, 9H), 0.86–0.82 (m, 23H), 0.71 (dd, $J = 10.4$, 3.6 Hz, 24H), 0.55–0.37 (m, 55H). ^{13}C NMR (101 MHz, $CDCl_3$): δ 159.9, 157.9, 141.7, 131.7, 130.4, 129.2, 128.5, 128.0, 121.2, 110.0, 105.1, 93.0, 77.2, 77.0, 76.8, 75.6, 68.7, 68.6, 35.6, 31.7, 31.6, 31.4, 29.3, 29.2, 29.0, 28.6, 28.5, 25.7, 25.5, 25.1, 22.6, 22.5, 22.2, 14.1, 14.0, 13.7. MALDI-MS (HRMS): m/z calcd. for $C_{203}H_{251}N_7O_{12}S_3Zn$: $[M]^+$ 3138.7699; found 3137.7694.

2.1.5 Procedure for synthesis of TZ5. To a solution of **4** (150 mg, 0.071 mmol) in THF (5 mL) was added tetra-n-butylammonium fluoride solution 1.0 M in THF (0.71 mL, 0.71

mmol). After stirring at room temperature for 10 min, the mixture was extracted with CH_2Cl_2/H_2O. The organic layer was collected and dried over Na_2SO_4, and the solvent was removed under vacuum to afford a crude product of desilylated porphyrin, which was used without further purification. Afterward, to a solution of the desilylated porphyrin, **14** (283 mg, 0.212 mmol), $Pd_2(dba)_3$ (32 mg, 0.035 mmol), $AsPh_3$ (86 mg, 0.283 mmol), and NEt_3 (1 mL, 7.19 mmol) in THF (5 mL) was heated at 85 °C for 12 h. After cooling to room temperature, the catalyst was removed with Celite, and the solvent was removed under reduced pressure. The residue was purified by column chromatography (silica gel) using CH_2Cl_2 as eluent to give **TZ5** (99 mg, 43%) as a red solid. ^{1}H NMR (400 MHz, CDCl$_3$): δ 9.55 (d, J = 4.7 Hz, 2H), 9.23 (d, J = 4.7 Hz, 2H), 8.82 (d, J = 4.5 Hz, 2H), 8.63 (d, J = 4.7 Hz, 2H), 8.19 (dd, J = 13.8, 8.6 Hz, 4H), 8.02 (s, 1H), 7.72 (d, J = 7.4 Hz, 1H), 7.66–7.61 (m, 3H), 7.57–7.50 (m, 3H), 7.31–7.28 (m, 10H), 7.15–7.11 (m, 12H), 6.94 (d, J = 8.7 Hz, 3H), 6.11 (s, 4H), 4.80 (s, 2H), 3.91–3.76 (m, 22H), 2.61–2.56 (m, 8H), 2.17 (d, J = 8.7 Hz, 2H), 1.77–1.71 (m, 5H), 1.62–1.54 (m, 68H), 1.44–1.40 (m, 10H), 1.36–1.24 (m, 54H), 1.19–1.15 (m, 18H), 1.00–0.94 (m, 9H), 0.86 (dd, J = 13.0, 6.9 Hz, 24H), 0.75–0.69 (m, 22H), 0.62–0.40 (m, 48H). ^{13}C NMR (101 MHz, CDCl$_3$): δ 159.9, 159.2, 157.9, 152.3, 151.5, 150.7, 150.3, 141.9, 141.8, 141.6, 131.7, 130.5, 128.5, 128.4, 128.0, 121.2, 110.0, 105.1, 93.0, 77.6, 77.2, 77.0, 76.8, 68.7, 68.6, 67.9, 35.6, 31.7, 31.6, 31.4, 31.3, 30.1, 29.3, 29.2, 29.1, 29.0, 28.6, 28.4, 26.6, 25.7, 25.5, 25.1, 22.6, 22.5, 22.2, 14.1, 14.0, 13.7. MALDI-MS (HRMS): m/z calcd. for $C_{211}H_{268}N_8O_{12}S_2Zn$: $[M]^+$ 3233.9340; found 3233.9334.

2.1.6 Procedure for synthesis of TZ6. To a solution of **1** (95 mg, 0.061 mmol) in THF (5 mL) was added tetra-n-butylammonium fluoride solution 1.0 M in THF (0.61 mL, 0.61 mmol). After stirring at room temperature for 10 min, the mixture was extracted with CH_2Cl_2/H_2O. The organic layer was collected and dried over Na_2SO_4, then the solvent was removed under a vacuum to afford a crude product of desilylated porphyrin, which was used without further purification. Afterward, to a solution of the desilylated porphyrin, **6** (40.0 mg, 0.18 mmol), $Pd_2(dba)_3$ (20 mg, 0.03 mmol), $AsPh_3$ (70 mg, 0.24 mmol), and NEt_3 (1.85 mL, 18.0 mmol) in THF (12 mL) were heated at 85 °C for 12 h. After cooling to room temperature, the catalyst was removed with Celite, and the solvent was removed under reduced pressure. The residue was purified by column chromatography (Silica gel) using CH_2Cl_2 as eluent to give **TZ6** (48 mg, 48%) as a brown solid. ^{1}H NMR (400 MHz, CDCl$_3$): δ 9.64 (d, J = 4.6 Hz, 2H), 9.17 (d, J = 4.6 Hz, 2H), 8.89 (d, J = 4.6 Hz, 2H), 8.68 (d, J = 4.6 Hz, 2H), 8.17 (d, J = 8.4 Hz, 2H), 8.07 (d, J = 8.2 Hz, 2H), 7.66 (t, J = 8.4 Hz, 2H), 7.20 (d, J = 8.6 Hz, 4H), 6.95 (dd, J = 13.0, 8.6 Hz, 8H), 3.84 (dd, J = 6.2, 4.3 Hz, 8H), 2.52–2.39 (m, 4H), 1.62–1.44 (m, 6H), 1.26 (s, 28H), 0.98 (dd, J = 13.6, 6.7 Hz, 10H), 0.93–0.74 (m, 20H), 0.74–0.55 (m, 28H), 0.48 (dt, J = 7.0, 6.1 Hz, 28H). ^{13}C NMR (101 MHz, CDCl$_3$): δ 159.9, 152.2, 152.0, 150.6, 150.4, 134.8, 132.4, 132.2, 131.9, 131.4, 130.7, 130.2, 129.9, 129.7, 128.8, 123.7, 122.0, 120.7, 114.8, 105.3, 95.1, 77.4, 77.1, 76.8, 68.7, 35.3, 32.3, 32.0, 31.8, 31.6, 31.5, 31.0, 29.8, 29.5, 29.2, 28.7, 28.7, 28.5, 28.3, 25.2, 25.1, 22.8,

22.7, 22.3, 14.2, 13.9. ESI-MS (HRMS): m/z calcd. for $C_{100}H_{122}N_6O_6Zn$: $[M]^+$ 1566.8712; found 1566.8693.

2.1.7 Procedure for synthesis of TZ7. To a solution of **4** (150 mg, 0.071 mmol) in THF (5 mL) was added tetra-n-butylammonium fluoride solution 1.0 M in THF (0.71 mL, 0.71 mmol). After stirring at room temperature for 10 min, the mixture was extracted with CH_2Cl_2/H_2O. The organic layer was collected and dried over Na_2SO_4. The solvent was removed under vacuum to afford a crude product of desilylated porphyrin, which was used without further purification. Afterward, to a solution of the desilylated porphyrin, **6** (40.0 mg, 0.18 mmol), $Pd_2(dba)_3$ (20 mg, 0.03 mmol), $AsPh_3$ (70 mg, 0.24 mmol), and NEt_3 (1.85 mL, 18.0 mmol) in THF (12 mL) were heated at 85 °C for 12 h. After cooling to room temperature, the catalyst was removed with Celite, and the solvent was removed under reduced pressure. The residue was purified by column chromatography (silica gel) using CH_2Cl_2 as eluent to give **TZ7** (25 mg, 48%) as a brown solid. ^{1}H NMR (400 MHz, CDCl$_3$): δ 9.61 (d, J = 4.6 Hz, 2H), 9.24 (d, J = 4.5 Hz, 2H), 8.88 (d, J = 4.6 Hz, 2H), 8.63 (d, J = 4.6 Hz, 2H), 8.14 (d, J = 7.8 Hz, 2H), 8.02 (d, J = 7.7 Hz, 2H), 7.65 (t, J = 8.4 Hz, 2H), 7.30 (d, J = 8.5 Hz, 4H), 7.14 (d, J = 8.5 Hz, 4H), 6.96 (d, J = 8.4 Hz, 4H), 6.12 (s, 4H), 3.90 (t, J = 6.6 Hz, 5H), 3.88–3.81 (m, 5H), 3.78 (t, J = 6.5 Hz, 14H), 1.82–1.66 (m, 6H), 1.56 (dd, J = 14.3, 6.7 Hz, 10H), 1.41 (d, J = 8.4 Hz, 5H), 1.38–1.11 (m, 44H), 0.99 (dd, J = 19.9, 13.4 Hz, 10H), 0.87 (dd, J = 9.5, 4.5 Hz, 8H), 0.83–0.68 (m, 26H), 0.68–0.48 (m, 35H), 0.44 (t, J = 7.3 Hz, 22H). ^{13}C NMR (101 MHz, CDCl$_3$): δ 159.9, 159.3, 158.0, 152.3, 152.1, 150.9, 150.4, 132.3, 131.9, 129.9, 126.0, 121.3, 120.9, 114.7, 113.4, 105.2, 93.0, 77.4, 77.3, 77.1, 76.8, 68.8, 68.0, 31.7, 31.5, 31.4, 29.8, 29.4, 29.1, 28.7, 28.5, 25.8, 25.6, 25.2, 22.7, 22.6, 22.3, 14.1, 13.9. MALDI-MS (HRMS): m/z calcd. for $C_{136}H_{178}N_6O_{12}Zn$: $[M]^+$ 2151.28; found 2151.30.

2.1.8 Procedure for synthesis of TZ8. To a solution of **1** (140 mg, 0.066 mmol) in THF (4.7 mL) was added tetra-n-butylammonium fluoride solution 1.0 M in THF (0.66 mL, 0.66 mmol). After stirring at room temperature for 10 min, the mixture was extracted with CH_2Cl_2/H_2O. The organic layer was collected, dried over Na_2SO_4, and the solvent was removed under vacuum to afford a crude product of desilylated porphyrin, which was used without further purification. Afterward, to a solution of the desilylated porphyrin, **7** (75.0 mg, 0.15 mmol), $Pd_2(dba)_3$ (46 mg, 0.05 mmol), $AsPh_3$ (123 mg, 0.4 mmol), and NEt_3 (2 mL, 20.0 mmol) in THF (5 mL) was heated at 85 °C for 12 h. After cooling to room temperature, the catalyst was removed with Celite, and the solvent was removed under reduced pressure. The residue was purified by column chromatography (silica gel) using CH_2Cl_2 as eluent to get crude as a brown solid. The crude was dissolved in chloroform (5 mL) and added 2-cyanoacetic acid (0.006 g, 0.06 mmol) and piperidine (0.02 mL, 0.13 mmol) and then reacted at 70 °C for 12 h. After cooling to room temperature, the mixture was added to acetic acid (5 mL) and extracted with CH_2Cl_2/H_2O. The solvent was removed under reduced pressure. The residue was purified by column chromatography (silica gel) using $CH_2Cl_2/EA = 4 : 1$ as eluent to give **TZ8** (41 mg, 78%) as a brown solid. ^{1}H NMR (400 MHz, CDCl$_3$): δ 9.57 (d, J =

4.5 Hz, 2H), 9.15 (d, J = 4.5 Hz, 2H), 8.88 (d, J = 4.5 Hz, 2H), 8.66 (d, J = 4.5 Hz, 2H), 8.25 (d, J = 3.8 Hz, 1H), 8.09–8.05 (m, 1H), 7.70–7.66 (m, 3H), 7.57 (dd, J = 32.0, 3.6 Hz, 2H), 7.45 (d, J = 7.6 Hz, 1H), 7.21 (d, J = 8.7 Hz, 4H), 7.00 (d, J = 8.5 Hz, 5H), 6.94 (d, J = 8.7 Hz, 5H), 4.91 (t, J = 7.1 Hz, 2H), 3.92–3.81 (m, 8H), 2.46 (t, J = 7.8 Hz, 4H), 2.34–2.27 (m, 3H), 1.70–1.44 (m, 18H), 1.43–1.14 (m, 116H), 1.12–1.10 (m, 20H), 1.08–0.93 (m, 20H), 0.93–0.77 (m, 69H), 0.74–0.51 (m, 53H). ^{13}C NMR (151 MHz, CDCl$_3$): δ 159.8, 159.7, 152.0, 151.7, 150.5, 150.4, 150.1, 134.6, 132.2, 131.9, 130.5, 130.3, 129.8, 128.7, 121.9, 120.9, 114.2, 105.4, 77.2, 77.0, 76.8, 68.8, 68.6, 38.7, 37.1, 35.2, 34.4, 32.7, 31.9, 31.8, 31.7, 31.6, 31.5, 31.4, 31.3, 30.4, 30.2, 30.0, 29.7, 29.5, 29.4, 29.2, 29.1, 29.0, 28.9, 28.7, 28.6, 28.4, 28.2, 28.1, 28.0, 27.1, 26.7, 25.1, 25.0, 24.8, 23.8, 23.0, 22.7, 22.6, 22.4, 22.3, 22.2, 19.7, 14.1, 13.9, 13.8, 13.7, 11.0. MALDI-TOF (HRMS): m/z calcd. for C$_{116}$H$_{141}$N$_9$O$_6$S$_2$Zn: [M]$^+$ 1883.9732; found 1883.9983.

2.1.9 Procedure for synthesis of TZ9. To a solution of **4** (140 mg, 0.070 mmol) in THF (4.7 mL) was added tetra-n-butylammonium fluoride solution 1.0 M in THF 0.66 mL, (0.66 mmol). After stirring at room temperature for 10 min, the mixture was extracted with CH$_2$Cl$_2$/H$_2$O. The organic layer was collected, dried over Na$_2$SO$_4$, and the solvent was removed under vacuum to afford a crude product of desilylated porphyrin, which was used without further purification. Afterward, to a solution of the desilylated porphyrin, **7** (52.0 mg, 0.105 mmol), Pd$_2$(dba)$_3$ (32 mg, 0.035 mmol), AsPh$_3$ (86 mg, 0.283 mmol), and NEt$_3$ (1 mL, 10.0 mmol) in THF (5 mL) were heated at 85 °C for 12 h. After cooling to room temperature, the catalyst was removed with Celite, and the solvent was removed under reduced pressure. The residue was purified by column chromatography (silica gel) using CH$_2$Cl$_2$ as eluent to get crude as a brown solid. The crude was dissolved in chloroform (5 mL) and added 2-cyanoacetic acid (0.006 g, 0.06 mmol) and piperidine (0.02 mL, 0.13 mmol) and then reacted at 70 °C for 12 h. After cooling to room temperature, the mixture was added to acetic acid (5 mL) and extracted with CH$_2$Cl$_2$/H$_2$O. The solvent was removed under reduced pressure. The residue was purified by column chromatography (silica gel) using CH$_2$Cl$_2$/EA = 4 : 1 as eluent to give **TZ9** (23 mg, 47%) as a brown solid. ^{1}H NMR (400 MHz, CDCl$_3$): δ 9.62 (d, J = 4.3 Hz, 2H), 9.29–9.23 (m, 2H), 8.86 (d, J = 4.5 Hz, 2H), 8.65 (dd, J = 15.5, 4.5 Hz, 2H), 8.16–8.09 (m, 2H), 7.81–7.78 (m, 1H), 7.72–7.66 (m, 2H), 7.61–7.75 (m, 3H), 7.51–7.46 (m, 2H), 7.30 (d, J = 8.5 Hz, 5H), 7.13 (d, J = 8.5 Hz, 4H), 6.98–6.92 (m, 4H), 6.11 (s, 4H), 4.81 (d, J = 8.4 Hz, 2H), 3.91–3.76 (m, 26H), 2.22–2.16 (m, 1H), 1.90–1.71 (m, 54H), 1.59–1.53 (m, 18H), 1.48–1.36 (m, 17H), 1.34–1.18 (m, 122H), 1.07–0.92 (m, 19H), 0.89–0.85 (m, 24H), 0.82–0.73 (m, 40H), 0.66–0.48 (m, 40H), 0.45–0.32 (m, 23H),. ^{13}C NMR (151 MHz, CDCl$_3$): δ 159.8, 159.2, 157.9, 152.2, 151.6, 150.8, 150.3, 150.2, 132.0, 131.7, 130.9, 130.1, 129.7, 125.8, 121.2, 120.9, 114.4, 113.3, 105.1, 92.9, 77.2, 77.0, 76.8, 68.7, 68.6, 67.9, 45.3, 37.1, 34.4, 31.9, 31.8, 31.6, 31.3, 30.1, 30.0, 29.7, 29.4, 29.3, 29.1, 29.0, 28.6, 28.5, 28.4, 27.1, 26.6, 25.7, 25.5, 25.1, 25.0, 23.0, 22.7, 22.6, 22.5, 22.2, 22.1, 19.7, 14.1, 14.0, 13.8, 8.6. MALDI-TOF (HRMS): m/z calcd. for C$_{152}$H$_{197}$N$_9$O$_{12}$S$_2$Zn: [M]$^+$ 2468.3809; found 2468.3563.

3. Results and discussions

3.1 Synthesis and characterization

The targeted **TZ** porphyrin dyes were synthesized following the route outlined in Scheme 1. The detailed procedures for each step are provided in the ESI.† Briefly, intermediates **1** and acceptor moieties with benzotriazole (**5**), cyanoacrylic acid derivatives (**6** and **7**), and benzothiadiazole (**8**) were prepared according to previously reported literature.[5,17,26,38–41] The synthetic approach involved desilylation of intermediate **1**, followed by Sonogashira coupling with acceptors **5** and **6** to afford final dyes **TZ1** and **TZ6**, respectively. For **TZ8** synthesis, the desilylated intermediate **1** was first reacted with compound **7**, followed by subsequent condensation with cyanoacetic acid. A modified bulky Hagfeldt donor **3** was prepared using established methods.[40] Key intermediate **4** was constructed via Buchwald–Hartwig amination of precursors **2** and **3**. Similar to the previously described approach, desilylation of compound **4** was followed by Sonogashira coupling with the corresponding acceptors (**5–8**, **11** and **14**) to furnish the target **TZ** dye series(**TZ2–TZ5**, **TZ7**, and **TZ9**) respectively This methodology enables systematic variation of both donor and acceptor units within the porphyrin framework, providing a versatile approach for tailoring the final dyes' properties.

3.2 Optical properties

The influence of various moieties on the light-harvesting properties of **TZ**-dyes was investigated through UV-vis spectroscopy in a tetrahydrofuran (THF) solution. As shown in Fig. 2, the UV-vis absorption spectra of **TZ** dyes reveal characteristic porphyrin Soret bands within the 400–550 nm range, accompanied by moderate-intensity Q bands spanning the 600–700 nm region. Among the **TZ** dyes series, **TZ1**, featuring an alkylamine donor and BTA acceptor, displays the highest extinction coefficient. **TZ2** incorporating BTD unit exhibits a broadened absorption spectrum with a bathochromic shift (400–540 and 620–720 nm) in the sorb and Q bands, respectively. This red-shifted absorption could be attributed to the reduced HOMO–LUMO energy gap due to the electron-withdrawing nature of the BTD moiety, which facilitated the absorption of lower-energy photons, consequently broadening the light-harvesting spectrum of the dye. Incorporation of the IDT unit in **TZ4** and **TZ5** results in the broadest absorption profile observed among **TZ** dyes series, encompassing a wide spectral range of the Soret band (390–588 nm) and Q band (622–694 nm). This extended light absorption arises from the well-established ability of IDT units to promote extended π-conjugation and enhance π-electron delocalization throughout the molecule. Moreover, the high extinction coefficient suggests the presence of strong ICT processes within these dyes.[42–44] Furthermore, the strategic placement of thiophene groups coupled with BTA in **TZ8** and **TZ9** allowed for the modulation of π-conjugation, offering valuable insights into fine-tuning light-harvesting properties. Consequently, these dyes exhibit a red-shifted and broadened absorption range, highlighting the influence of the thiophene group as a spacer on their light-capture profiles.
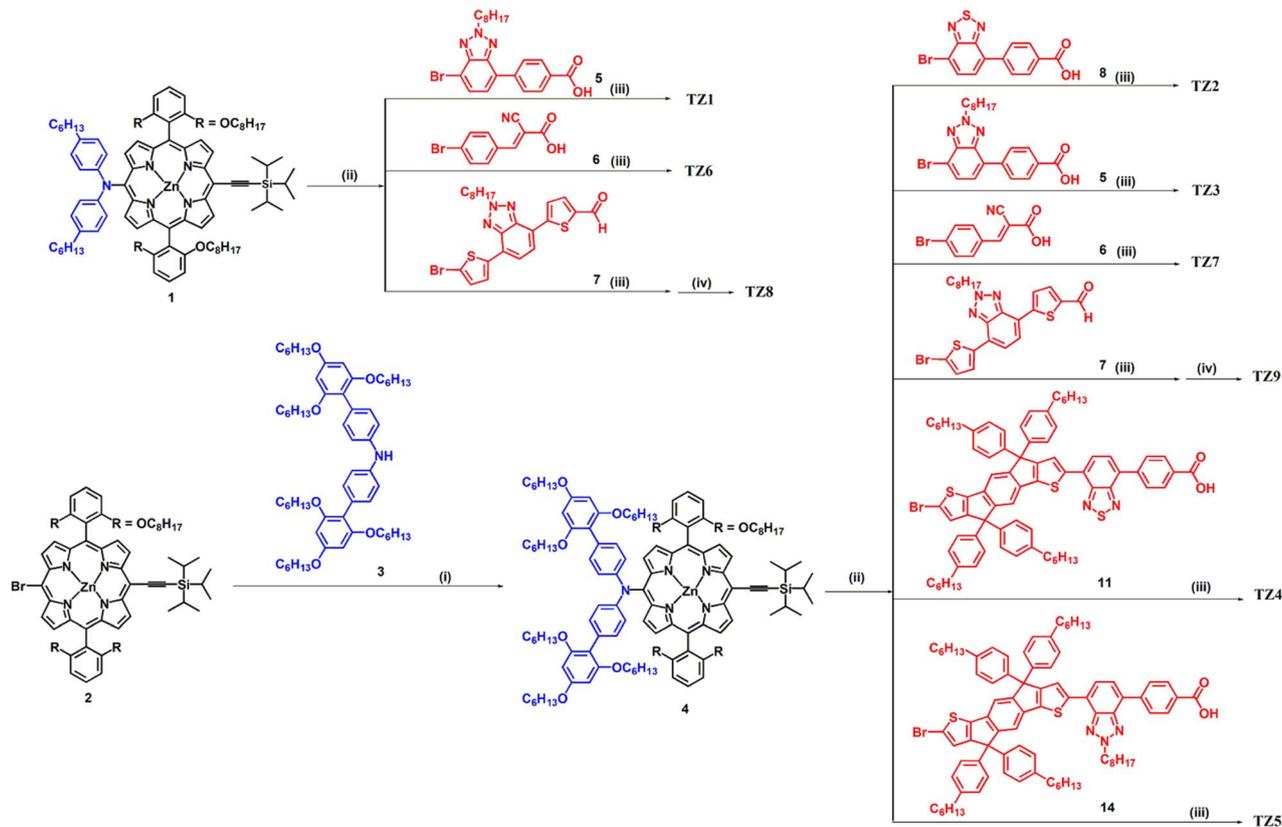
Scheme 1 Synthetic routes of **TZ** porphyrin dyes. (i) Pd (OAc)$_2$, NaOtBu, P(tBu)$_3$, toluene. (ii) tetra-n-Butylammonium fluoride (TBAF), THF. (iii) Pd$_2$(dba)$_3$, AsPh$_3$, Et$_3$N, THF. (iv) 2-cyanoacetic acid, piperidine, CHCl$_3$.

Steady-state fluorescence spectra were recorded in THF (Fig. S35†). A slight redshift in the fluorescence maximum of **TZ2** was observed, consistent with the trend evident in the absorption spectra. Furthermore, time-resolved fluorescence measurements were conducted using time-correlated single-photon counting (TCSPC) (Fig. S36†), and the average fluorescence lifetimes (τ) are summarized in Table 1. Notably, **TZ4** and **TZ5** exhibited longer lifetimes, suggesting their effectiveness in mitigating dye aggregation in dilute solutions.[45]

3.3 Electrochemical properties

Cyclic voltammetry was employed in a three-electrode configuration to investigate the electrochemical behaviours of **TZ** dyes. The electrochemical cell encompassed dry THF, TBAPF$_6$ as a supporting electrolyte, and ferrocene/ferrocenium as an internal reference electrode (Fig. S37†). Potentials obtained *versus* Fc$^+$/Fc redox couple were meticulously converted to the NHE scale by adding +0.63 V. E$_{HOMO}$ was estimated using the
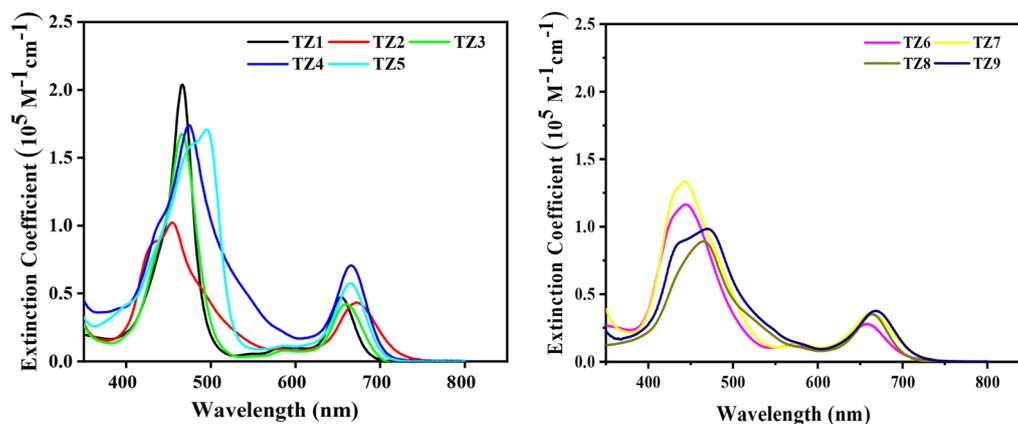

Fig. 2 UV-vis absorption spectra of **TZ** dyes in THF.

Table 1 Optical and electrochemical properties of **TZ** dyes in THF

Dye	Absorption[a] λ_{max} (nm) [$\varepsilon/10^4$ M^{-1} cm^{-1}]	Emission λ_{max} (nm)	τ_{AV}[b] (ns)	E_{ox}[c] [V]	E_{0-0}[d] [eV]	E_{S1}[e] V	ΔG_{inj}[f] (eV)	ΔG_{reg}[j] (eV)
TZ1	466 (2.0), 654 (0.5)	678	1.56	+0.80	1.86	−1.06	0.56	0.24
TZ2	435 (0.6), 454 (1.0), 772 (0.4)	731	1.54	+0.66	1.77	−1.11	0.61	0.10
TZ3	466 (1.7), 660 (0.4)	691	1.50	+0.67	1.84	−1.17	0.67	0.11
TZ4	474 (1.7), 666 (0.7)	702	2.00	+0.66	1.81	−1.15	0.65	0.10
TZ5	478 (1.6), 495 (1.7), 666 (0.6)	690	2.05	+0.68	1.83	−1.15	0.65	0.12
TZ6	442 (1.16), 659 (0.28)	677	1.26	+0.85	1.86	−1.01	0.51	0.29
TZ7	444 (1.13), 662 (0.34)	694	1.09	+0.75	1.83	−1.08	0.58	0.19
TZ8	465 (0.89), 664 (0.35)	684	1.15	+0.80	1.83	−1.03	0.52	0.24
TZ9	471 (0.98), 666 (0.37)	696	1.00	+0.70	1.81	−1.11	0.61	0.14

[a] Wavelength maximum for absorption and emission are recorded in THF at 25 °C. [b] Average fluorescence decays lifetimes of dyes in THF solution (1×10^{-6} M). [c] The oxidation potentials were determined by cyclic CV in THF containing 0.1 M tetrabutylammonium hexafluorophosphate (TBAPF$_6$) as electrolyte and were calibrated with ferrocene/ferrocenium (Fc/Fc$^+$) as internal reference at 25 °C and corrected to NHE by adding +0.63 V. [d] E_{0-0} were determined from the intersection of normalized absorption and emission spectra in THF. [e] Calculated by the following equation: $E_{S1} = E_{HOMO} - E_{0-0}$. [f] Driving force for electron injection from the S$^+$/S* to the CB of TiO$_2$ (−0.5 V vs. NHE). [j] Driving force for dye regeneration (cobalt redox electrolyte) (0.56 V vs. NHE).

redox potential ($E_{1/2(ox)}$) of the first oxidation, while the first excited states of **TZ** dyes were calculated by eqn (1):

$$E_{LUMO} = E_{HOMO} - E_{0-0} \qquad (1)$$

As shown in Fig. 3, incorporating alkoxy chains into the donor (modified Hagfeldt donor) upshifts the oxidation potential. It resulted in a narrowed band gap for **TZ2**, **TZ3**, **TZ4**, **TZ5**, **TZ7**, and **TZ9** compared to **TZ1**, **TZ6**, and **TZ8** (alkylamine-based donor). This could be ascribed to the augmented electron-donating propensity of the modified Hagfeldt donor, which promotes a more stable oxidized state and leads to a narrower band gap. Notably, **TZ2**, equipped with the strong electron-withdrawing BTD unit, exhibits the narrowest energy band gap among all dyes (1.77 eV). This suggests that the combined influence of the modified Hagfeldt and BTD units optimizes the electronic landscape for efficient light harvesting. Furthermore, employing thiophene groups coupled with BTA as a spacer in **TZ8** and **TZ9** results in narrower band gaps than their counterparts **TZ6** and **TZ7**. As demonstrated by UV-vis and CV measurements, the targeted manipulation of the molecular

architecture emerges as a critical strategy in fine-tuning the optoelectronic properties of **TZ** dyes.

3.4 Photovoltaic performance

The photovoltaic performance of DSSCs incorporating **TZ** dyes was examined under simulated AM 1.5G illumination. The resulting current density–voltage (J–V) curves and incident photon-to-current efficiency (IPCE) spectra are presented in Fig. 4. Detailed descriptions of device fabrication and measurement procedures are included in the ESI.† As shown in Table 2, devices incorporating **TZ2**–**TZ5** dyes exhibited reduced dye-loading capacities compared to **TZ1**. This disparity could be attributed to the steric hindrance imposed by the bulkier molecular structures of **TZ2**–**TZ5**, which impeded the efficient adsorption of dye molecules onto the TiO$_2$ surface. Consequently, the devices incorporating **TZ2**–**TZ5** exhibited lower J_{SC} than the **TZ1**-based device, following the **TZ1** > **TZ2** > **TZ3** > **TZ4** > **TZ5** trend. Moreover, the observed superiority in J_{SC} for **TZ1** could be ascribed to its enhanced driving force for dye regeneration (0.24 eV) compared to **TZ2**–**TZ5** ($\simeq 0.11$ eV), as elucidated by CV measurements and shown in Table 1.[46–50] Notably, **TZ4** and **TZ5**, incorporating the IDT moiety, displayed significantly higher V_{OC} of 0.863 V and 0.883 V, respectively, exceeding all other **TZ** dyes, despite lower dye-loading capacities. This superior ability to suppress charge recombination at the TiO$_2$ photoanode–electrolyte interface is attributed to the steric hindrance effect caused by the bulky IDT unit. On the other hand, although **TZ8** and **TZ9** demonstrated the highest dye-loading capacities, they showed low PCEs of 2.1% and 3.5%, respectively. This relatively low performance could be attributed to their elongated molecular structures, which promote intermolecular π–π interactions and increase dye aggregation. As shown in Fig. S38†, upon application to a 2 μm thick TiO$_2$ electrode, **TZ8** and **TZ9** exhibited significant blue shifts of 31 nm and 34 nm, respectively, whereas **TZ1** displayed a comparatively smaller blue shift of 12 nm. Furthermore, the elongated molecular structures of **TZ8** and **TZ9** may facilitate
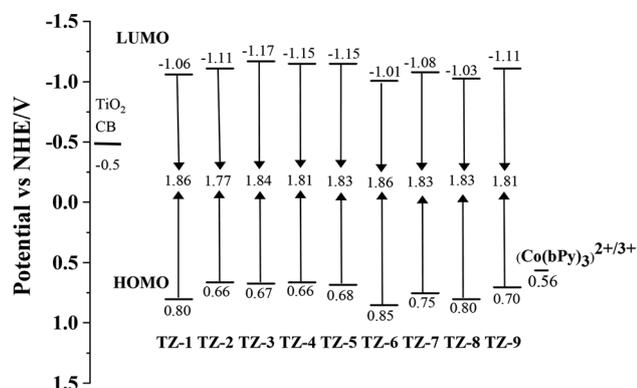

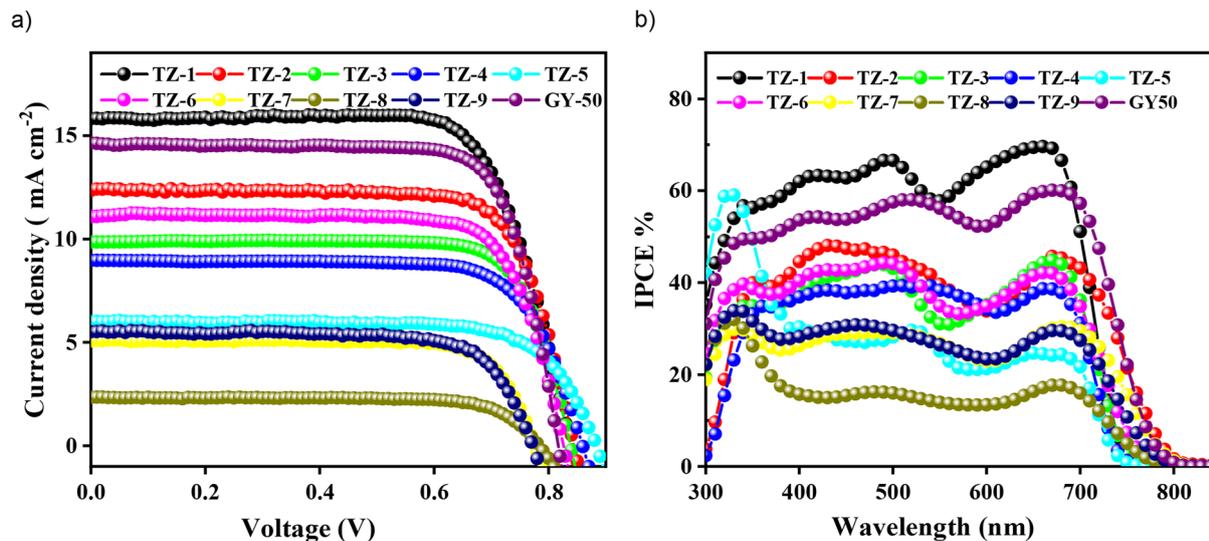**Fig. 3** Energy levels diagram of **TZ** dyes based on their optical and electrochemical data.

Fig. 4 (a) J–V curves under 1 sun illumination. (b) IPCE spectra of **TZ** dyes and **GY50**-based devices.

a larger tilt angle, potentially enhancing charge recombination (low V_{OC}), thereby negating the potential benefits of increased light harvesting achieved by the extended structures.[6,51–53]

IPCE spectra were employed to further elucidate the light-harvesting capability of the **TZ** dyes, as presented in Fig. 4b. All investigated dyes displayed characteristic IPCE profiles with two maxima around 480 nm and 700 nm, corresponding to the Soret and Q-band absorption transitions, respectively, with a minor dip observed at approximately 600 nm. The plateau heights in the IPCE spectra follow the trend: **TZ1** > **TZ2** > **TZ6** > **TZ3** > **TZ4** > **TZ5** > **TZ7** ≈ **TZ9** > **TZ8**. This trend is mirrored in the integrated Jsc values derived from the IPCE spectra, which closely correlate with the Jsc values obtained from the J–V curves, as summarized in Table 2. **TZ1** displays a superior IPCE value of 65%, surpassing its counterparts and the benchmark **GY50** dye (60%). The superiority of **TZ1** could be ascribed to the combination of dye loading capacity, the larger driving force for dye regeneration, and the higher extinction coefficient. On the other hand, **TZ7**, **TZ8**, and **TZ9** showed lower IPCE values due to

the dye aggregation and limitations in charge collection efficiency, as will be investigated using electrochemical impedance spectroscopy.

3.5 Electrochemical impedance spectroscopy study (EIS)

EIS under varying applied potential biases in darkness was employed to investigate the charge collection efficiency (η_{coll}), charge recombination resistance (R_{CT}) at the dye/TiO$_2$/electrolyte interface, and charge transport resistance (R_T). As shown in Fig. 5a, **TZ2**–**TZ5**-based devices exhibit comparable R_{CT} to **TZ1** despite a lower dye loading, suggesting that strategic bulking of the dye structures suppresses charge recombination through steric hindrance effects. Conversely, **TZ8** and **TZ9** display the lowest R_{CT} despite having the highest dye loading, which can be attributed to dye aggregation.

Consequently, these devices exhibited lower V_{OC} values (0.78–0.79 V, respectively). Notably, the DSSCs-based **TZ1** dye shows the lowest R_T values, as illustrated in Fig. 5b, consistent with its high

Table 2 Photovoltaic parameters of DSSCs-based on **TZ** and **GY50** under AM 1.5G illumination

Dye[a]	J_{SC} [mA cm^{-2}]	V_{OC} [V]	FF	PCE %	J_{SC}^{IPCE} [mA cm^{-2}]	Dye loading[b] [10^{-8} mol cm^{-2}]
TZ1	15.675 (15.512 ± 0.163)	0.834 (0.826 ± 0.008)	0.758 (0.738 ± 0.014)	9.909 (9.456 ± 0.439)	14.872	6.70
TZ2	12.351 (12.078 ± 0.272)	0.844 (0.846 ± 0.003)	0.759 (0.756 ± 0.003)	7.921 (7.738 ± 0.182)	11.655	4.52
TZ3	9.774 (9.702 ± 0.072)	0.845 (0.845 ± 0.00)	0.785 (0.775 ± 0.010)	6.480 (6.356 ± 0.124)	8.976	3.50
TZ4	9.001 (8.885 ± 0.116)	0.862 (0.859 ± 0.003)	0.746 (0.728 ± 0.018)	5.789 (5.556 ± 0.233)	8.495	3.10
TZ5	5.997 (5.638 ± 0.358)	0.883 (0.872 ± 0.011)	0.736 (0.743 ± 0.007)	3.901 (3.650 ± 0.251)	5.412	2.94
TZ6	11.031 (10.825 ± 0.206)	0.826 (0.824 ± 0.002)	0.770 (0.772 ± 0.002)	7.022 (6.901 ± 0.121)	10.331	8.25
TZ7	5.086 (4.911 ± 0.175)	0.776 (0.777 ± 0.001)	0.773 (0.771 ± 0.002)	3.055 (2.943 ± 0.112)	4.484	7.55
TZ8	2.344 (2.168 ± 0.176)	0.783 (0.786 ± 0.003)	0.753 (0.738 ± 0.015)	1.384 (1.258 ± 0.126)	1.976	10.10
TZ9	5.513 (5.251 ± 0.262)	0.772 (0.770 ± 0.002)	0.732 (0.745 ± 0.014)	3.116 (3.015 ± 0.101)	4.895	8.15
GY50	14.737 (14.779 ± 0.042)	0.817 (0.815 ± 0.002)	0.764 (0.757 ± 0.007)	9.207 (9.133 ± 0.074)	13.812	6.91

[a] Photovoltaic parameters were obtained from the champion cells. Averaged values of four independent cells with standard errors are presented in parentheses. [b] The values were obtained by averaging four independent cells.
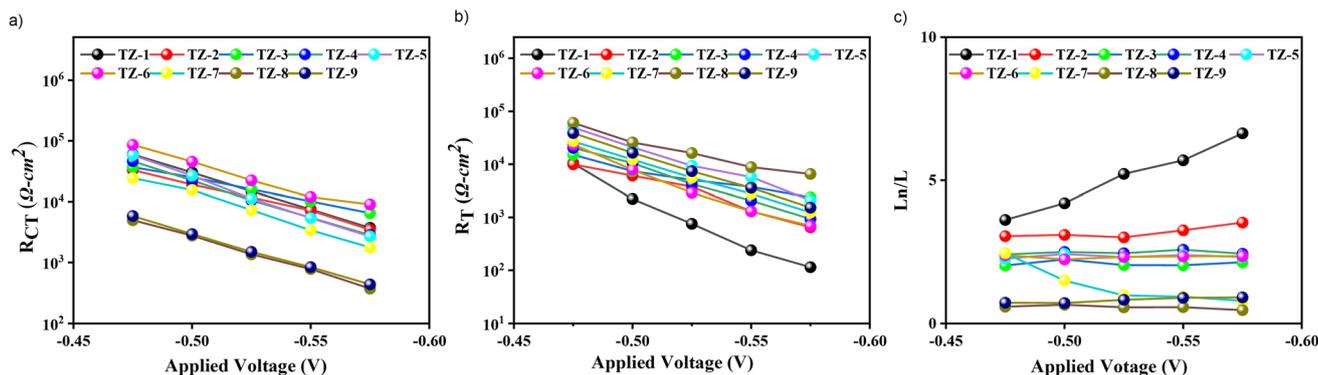
Fig. 5 (a) Logarithmic dependence of charge–recombination resistance. (b) Logarithmic dependence of charge–transport resistance. (c) Charge collection efficiency was calculated by L_n/L ratio.
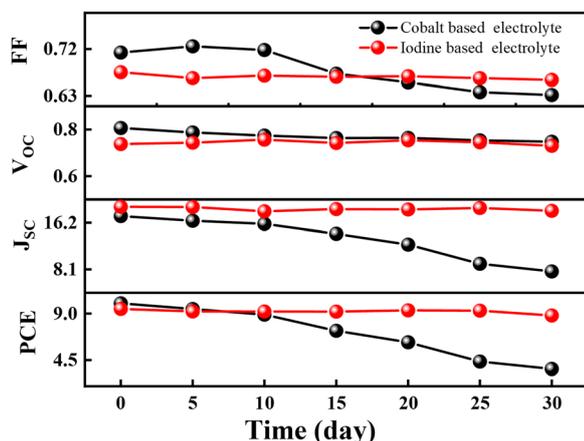

Fig. 6 Stability trail **TZ1**-based DSSCs using cobalt and iodine-based electrolytes at 60 °C.

J_{SC}. Conversely, the elevated R_T observed in the **TZ8**-based DSSC may be attributed to dye aggregation phenomena. This aggregation could impede efficient charge injection, which is consistent with the observed low J_{SC}. Finally, η_{coll} can be quantified using the equation $L_n/L = (R_{CT}/R_T)^{1/2}$, where L denotes TiO$_2$ thickness, and L_n represents the electron diffusion length. For efficient charge collection, the L_n/L ratio should exceed unity. As shown in Fig. 5c, **TZ7**, **TZ8**, and **TZ9** exhibit lower charge collection efficiencies, providing further evidence for their lower J_{SC}, V_{OC}, and, consequently, lower PCE values. Overall, among the investigated dyes, **TZ1**-based DSSC exhibited the highest PCE of 9.90%, outperforming both the other **TZ** dyes and **GY50** (PCE of 9.20%) under similar fabrication conditions. Conversely, **TZ7**–**TZ9** displayed lower PCEs (3.98%, 1.29%, and 3.52%, respectively) due to insufficient η_{coll} and increased dye aggregation.

3.6 Stability studies of TZ dyes

The photostability of **TZ** dyes was investigated by subjecting dye-coated nanocrystalline TiO$_2$ films to 1 sun illumination for a day. As illustrated in Fig. S39,† the UV-vis absorption spectra of the dyes showed a slight decrease, demonstrating their photostability.[54] Moreover, ^{1}H NMR analysis of powdered dyes

after 24 hours of continuous illumination (Fig. S40 and S41† for **TZ4** and **TZ5** as representative examples) confirmed their structural integrity under prolonged light exposure.

To assess thermal stability, thermogravimetric analysis (TGA) was employed. As presented in Fig. S42,† all **TZ** derivatives exhibited remarkable thermal stability, remaining stable up to 300 °C. To evaluate long-term device performance, DSSCs based on **TZ1** were subjected to aging tests at 60 °C for 30 days, utilizing both cobalt- and iodide-based electrolytes in 3-methoxypropionitrile (MPN). As depicted in Fig. 6, devices employing the iodide-based electrolyte outperformed cobalt-based devices, retaining 92% of their initial PCE compared to only 36%. This disparity could be attributed to the lower volatility of the iodide-based DSSCs.[6]

Furthermore, under continuous indoor illumination at 6000 lux, **TZ1**-based DSSCs maintained 93% and 76% of their initial PCE for iodine and cobalt-based electrolytes, respectively (Fig. S43 and Table S1†). The combination of high thermal and photostability, coupled with acceptable durability, particularly under dim light conditions, positions **TZ** dyes as promising candidates for practical solar energy conversion applications.

4. Conclusion

This study meticulously described the design, synthesis, and performance evaluation of nine novel porphyrin sensitizers, designated as **TZ** dyes, for the application in DSSCs. A systematic investigation was undertaken to explore the structure–performance relationship of these sensitizers. By strategically modifying the donor, π-spacer, and acceptor units, we aimed to understand the critical interplay between molecular design and photovoltaic efficiency. Incorporating a bulky modified Hagfeldt donor resulted in a red-shifted absorption spectrum compared to their counterparts containing alkylamine-based donors. Furthermore, introducing IDT units as π-spacer n **TZ4** and **TZ5** led to enhanced LHE and demonstrably suppressed the charge recombination through steric hindrance effects. These combined effects translated to high V_{OC} values for **TZ4** and **TZ5**. However, this approach comes at the cost of a lower dye loading capacity, consequently leading to a diminished J_{SC}. Further

extension of the π-spacer with thiophene and benzothiadiazole (BTA) moieties in **TZ8** and **TZ9** further red-shifted the absorption spectrum however, it increased the dye aggregation, limiting their photovoltaic performance. All **TZ** dye derivatives exhibited remarkable thermal stability, demonstrating robust structural integrity up to 300 °C. Moreover, these dyes displayed excellent photochemical stability.

Among the investigated dyes, DSSCs based on **TZ1** exhibited a remarkable PCE of 9.90%% ($J_{SC} = 15.675$ mA cm^{-2}, $V_{OC} = 0.834$ V, and FF = 0.758), surpassing the PCE of 9.20% ($J_{SC} = 14.737$ mA cm^{-2}, $V_{OC} = 0.817$ V, and FF = 0.764) achieved by the benchmark **GY50** under identical fabrication. Furthermore, the exceptional thermal and photochemical stability of **TZ1**, coupled with its promising long-term operational stability, underscores its potential for practical application in sustainable solar energy conversion technologies.

Data availability

The data supporting this article have been included as part of the ESI.†

Conflicts of interest

There are no conflicts to declare.

Acknowledgements

References

1 M. Grätzel, *Nature*, 2001, **414**, 338–344.

2 P. Szuromi, B. Jasny, D. Clery, J. Austin and B. Hanson, *Science*, 2007, **315**, 781.

3 A. Costello, M. Abbas, A. Allen, S. Ball, S. Bell, R. Bellamy, S. Friel, N. Groce, A. Johnson, M. Kett, M. Lee, C. Levy, M. Maslin, D. McCoy, B. McGuire, H. Montgomery, D. Napier, C. Pagel, J. Patel, J. A. P. deOliveira, N. Redclift, H. Rees, D. Rogger, J. Scott, J. Stephenson, J. Twigg, J. Wolff and C. Patterson, *Lancet*, 2009, **373**, 1693–1733.

4 J. Rogelj, M. DenElzen, N. Höhne, T. Fransen, H. Fekete, H. Winkler, R. Schaeffer, F. Sha, K. Riahi and M. Meinshausen, *Nature*, 2016, **534**, 631–639.

5 Y. S. Tingare, N. S. N. Vinh, H.-H. Chou, Y.-C. Liu, Y.-S. Long, T.-C. Wu, T.-C. Wei and C.-Y. Yeh, *Adv. Energy Mater.*, 2017, **7**, 1700032.

6 C.-C. Chen, V. S. Nguyen, H.-C. Chiu, Y.-D. Chen, T.-C. Wei and C.-Y. Yeh, *Adv. Energy Mater.*, 2022, **12**, 2104051.

7 C. Teng, X. Yang, C. Yang, S. Li, M. Cheng, A. Hagfeldt and L. Sun, *J. Phys. Chem. C*, 2010, **114**, 9101–9110.

8 A. Hagfeldt, G. Boschloo, L. Sun, L. Kloo and H. Pettersson, *Chem. Rev.*, 2010, **110**, 6595–6663.

9 Y. Xie, Y. Tang, W. Wu, Y. Wang, J. Liu, X. Li, H. Tian and W. H. Zhu, *J. Am. Chem. Soc.*, 2015, **137**, 14055–14058.

10 M. Grätzel, *Acc. Chem. Res.*, 2009, **42**, 1788–1798.

11 S. Venkatesan, T.-H. Hsu, H. Teng and Y.-L. Lee, *Sol. RRL*, 2023, **7**, 2300220.

12 F. A. Faraghally, A. F. Musa, C.-C. Chen, Y.-H. Chen, Y.-D. Chen, C.-Y. Yeh and T.-C. Wei, *Small Struct.*, 2024, **5**, 2400236.

13 M. Grätzel, in *Pure and Applied Chemistry*, Walter de Gruyter GmbH, 2001, vol. 73, pp. 459–467.

14 M. Grätzel, *J. Photochem. Photobiol. C Photochem. Rev.*, 2003, **4**, 145–153.

15 S. Huang, Q. Li, S. Li, C. Li, H. Tan and Y. Xie, *Chem. Commun.*, 2024, **60**, 4521–4536.

16 J. M. Ji, H. Zhou and H. K. Kim, *J. Mater. Chem. A*, 2018, **6**, 14518–14545.

17 A. Yella, C.-L. Mai, S. M. Zakeeruddin, S. N. Chang, C.-H. Hsieh, C.-Y. Yeh and M. Grätzel, *Angew. Chem. Int. Ed.*, 2014, **53**, 2973–2977.

18 S. H. Kang, I. T. Choi, M. S. Kang, Y. K. Eom, M. J. Ju, J. Y. Hong, H.-S. Kang and H. K. Kim, *J. Mater. Chem. A*, 2013, **1**, 3977–3982.

19 C. Yi, F. Giordano, N. LeCevey-Ha, H. N. Tsao, S. M. Zakeeruddin and M. Grätzel, *ChemSusChem*, 2014, **7**, 1107–1113.

20 M. Ishida, D. Hwang, Z. Zhang, Y. J. Choi, J. Oh, V. M. Lynch, D. Y. Kim, J. L. Sessler and D. Kim, *ChemSusChem*, 2015, **8**, 2967–2977.

21 S. H. Kang, M. J. Jeong, Y. K. Eom, I. T. Choi, S. M. Kwon, Y. Yoo, J. Kim, J. Kwon, J. H. Park and H. K. Kim, *Adv. Energy Mater.*, 2017, **7**, 1602117.

22 Z. Li, Q. Li, C. Li and Y. Xie, *Mater. Chem. Front.*, 2023, **8**, 652–680.

23 J. E. Kroeze, N. Hirata, S. Koops, M. K. Nazeeruddin, L. Schmidt-Mende, M. Grätzel and J. R. Durrant, *J. Am. Chem. Soc.*, 2006, **128**, 16376–16383.

24 N. Koumura, Z. S. Wang, S. Mori, M. Miyashita, E. Suzuki and K. Hara, *J. Am. Chem. Soc.*, 2006, **128**, 14256–14257.

25 A. Yella, H.-W. W. Lee, H. N. Tsao, C. Yi, A. K. Chandiran, M. K. Nazeeruddin, E. W.-G. Diau, C.-Y. Yeh, S. M. Zakeeruddin and M. Grätzel, *Science*, 2011, **334**, 629–634.

26 S. Mathew, A. Yella, P. Gao, R. Humphry-Baker, B. F. E. Curchod, N. Ashari-Astani, I. Tavernelli, U. Rothlisberger, M. K. Nazeeruddin and M. Grätzel, *Nat. Chem.*, 2014, **6**, 242–247.

27 T. Ripolles-Sanchis, B. C. Guo, H. P. Wu, T. Y. Pan, H. W. Lee, S. R. Raga, F. Fabregat-Santiago, J. Bisquert, C.-Y. Yeh and E. W.-G. Diau, *Chem. Commun.*, 2012, **48**, 4368–4370.

28 H.-Y. Hsu, H.-C. Chiang, J.-Y. Hu, K. Awasthi, C.-L. Mai, C.-Y. Yeh, N. Ohta and E. W.-G. Diau, *J. Phys. Chem. C*, 2013, **117**, 24761–24766.

29 M. R. DiNunzio, B. Cohen, S. Pandey, S. Hayse, G. Piani and A. Douhal, *J. Phys. Chem. C*, 2014, **118**, 11365–11376.

30 J. Luo, Z. Xie, J. Zou, X. Wu, X. Gong, C. Li and Y. Xie, *Chin. Chem. Lett.*, 2022, **33**, 4313–4316.

31 J. Zou, Y. Wang, G. Baryshnikov, J. Luo, X. Wang, H. Ågren, C. Li and Y. Xie, *ACS Appl. Mater. Interfaces*, 2022, **14**, 33274–33284.

32 L. Schmidt-Mende, W. M. Campbell, Q. Wang, K. W. Jolley, D. L. Officer, M. K. Nazeeruddin and M. Grätzel, *ChemPhysChem*, 2005, **6**, 1253–1258.

33 Q. Wang, W. M. Campbell, E. E. Bonfantani, K. W. Jolley, D. L. Officer, P. J. Walsh, K. Gordon, R. Humphry-Baker, M. K. Nazeeruddin and M. Grätzel, *J. Phys. Chem. B*, 2005, **109**, 15397–15409.

34 W. M. Campbell, K. W. Jolley, P. Wagner, K. Wagner, P. J. Walsh, K. C. Gordon, L. Schmidt-Mende, M. K. Nazeeruddin, Q. Wang, M. Grätzel and D. L. Officer, *J. Phys. Chem. C*, 2007, **111**, 11760–11762.

35 S. L. Wu, H. P. Lu, H. T. Yu, S. H. Chuang, C. L. Chiu, C. W. Lee, E. W.-G. Diau and C. Y. Yeh, *Energy Environ. Sci.*, 2010, **3**, 949–955.

36 C.-W. Lee, H.-P. Lu, C.-M. Lan, Y.-L. Huang, Y.-R. Liang, W.-N. Yen, Y.-C. Liu, Y.-S. Lin, E. W.-G. Diau and C.-Y. Yeh, *Chem.–Eur. J.*, 2009, **15**, 1403–1412.

37 T. Bessho, S. M. Zakeeruddin, C.-Y. Yeh, E. W.-G. Diau and M. Grätzel, *Angew. Chem., Int. Ed.*, 2010, **49**, 6646–6649.

38 C.-C. Chen, J.-S. Chen, V. S. Nguyen, T.-C. Wei and C.-Y. Yeh, *Angew. Chem.*, 2021, **133**, 4936–4943.

39 C.-C. Chen, Y.-H. Chen, V. S. Nguyen, S.-Y. Chen, M.-C. Tsai, J.-S. Chen, S.-Y. Lin, T.-C. Wei and C.-Y. Yeh, *Adv. Energy Mater.*, 2023, **13**, 2300353.

40 Y.-H. Chen, C.-C. Chen, V. S. Nguyen, M.-N. Lu, Y.-D. Chen, Y.-C. Lin, T.-C. Wei and C.-Y. Yeh, *ACS Appl. Energy Mater.*, 2022, **5**, 13544–13553.

41 J. M. Ji, H. Zhou, Y. K. Eom, C. H. Kim and H. K. Kim, *Adv. Energy Mater.*, 2020, **10**, 2000124.

42 Y. Li, K. Yao, H. L. Yip, F. Z. Ding, Y. X. Xu, X. Li, Y. Chen and A. K. Y. Jen, *Adv. Funct. Mater.*, 2014, **24**, 3631–3638.

43 Y.-X. Xu, C.-C. Chueh, H.-L. Yip, F.-Z. Ding, Y.-X. Li, C.-Z. Li, X. -Li, W.-C. Chen and A. K.-Y. Jen, *Adv. Mater.*, 2012, **24**, 6356–6361.

44 Y. Liu, Y. Cao, W. Zhang, M. Stojanovic, M. I. Dar, P. Péchy, Y. Saygili, A. Hagfeldt, S. M. Zakeeruddin and M. Grätzel, *Angew. Chem., Int. Ed.*, 2018, **57**, 14125–14128.

45 Y. Zhang, T. Higashino, I. Nishimura and H. Imahori, *ACS Appl. Mater. Interfaces*, 2024, **16**, 67761–67770.

46 S. Hattori, Y. Wada, S. Yanagida and S. Fukuzumi, *J. Am. Chem. Soc.*, 2005, **127**, 9648–9654.

47 S. M. Feldt, G. Wang, G. Boschloo and A. Hagfeldt, *J. Phys. Chem. C*, 2011, **115**, 21500–21507.

48 M. Hussain, A. Islam, I. Bedja, R. K. Gupta, L. Han and A. El-Shafei, *Phys. Chem. Chem. Phys.*, 2014, **16**, 14874–14881.

49 Y. Saygili, M. Söderberg, N. Pellet, F. Giordano, Y. Cao, A. B. Munoz-García, S. M. Zakeeruddin, N. Vlachopoulos, M. Pavone, G. Boschloo, L. Kavan, J. E. Moser, M. Grätzel, A. Hagfeldt and M. Freitag, *J. Am. Chem. Soc.*, 2016, **138**, 15087–15096.

50 M. Hu, J. Shen, Z. Yu, R. Z. Liao, G. G. Gurzadyan, X. Yang, A. Hagfeldt, M. Wang and L. Sun, *ACS Appl. Mater. Interfaces*, 2018, **10**, 30409–30416.

51 H. Imahori, S. Kang, H. Hayashi, M. Haruta, H. Kurata, S. Isoda, S. E. Canton, Y. Infahsaeng, A. Kathiravan, T. Pascher, P. Chábera, A. P. Yartsev and V. Sundström, *J. Phys. Chem. A*, 2011, **115**, 3679–3690.

52 S. Ye, A. Kathiravan, H. Hayashi, Y. Tong, Y. Infahsaeng, P. Chabera, T. Pascher, A. P. Yartsev, S. Isoda, H. Imahori and V. Sundström, *J. Phys. Chem. C*, 2013, **117**, 6066–6080.

53 C.-C. Chen, J.-S. Chen, V. S. Nguyen, T.-C. Wei and C.-Y. Yeh, *Angew. Chem. Int. Ed.*, 2021, **60**, 4886–4893.

54 Y. Wang, B. Chen, W. Wu, X. Li, W. Zhu, H. Tian and Y. Xie, *Angew. Chem., Int. Ed.*, 2014, **126**, 10955–10959.